

Vigilance Estimation Using a Wearable EOG Device in Real Driving Environment

Wei-Long Zheng¹, Student Member, IEEE, Kunpeng Gao, Gang Li¹, Wei Liu, Chao Liu, Jing-Quan Liu¹,
Guoxing Wang¹, Senior Member, IEEE, and Bao-Liang Lu¹, Senior Member, IEEE

Abstract—Vigilance decrement in driving tasks has been reported to be a major factor in fatal accidents and could severely endanger public transportation safety. However, efficient approaches for estimating vigilance in real driving environment are still lacking. In this paper, we propose a novel approach for implementing continuous vigilance estimation using forehead electrooculograms (EOGs) acquired by wearable dry electrodes in both simulated and real driving environments. To improve the feasibility of this approach for real-world applications, a forehead EOG-based electrode placement with only four electrodes is designed. Flexible dry electrodes and an acquisition board are integrated as a wearable device for recording EOGs. Twenty and ten subjects participated in the simulated and real-world driving environment experiments, respectively. Accurate eye movement parameters from eye-tracking glasses are extracted to calculate the PERCLOS index for vigilance annotation. This is because the vigilance state is a temporally dynamic process, and a continuous conditional random field and a continuous conditional neural field are introduced to construct more accurate vigilance estimation models. To evaluate the efficiency of our system, systematic experiments are performed in real scenarios under various illumination and weather conditions following laboratory simulations as preliminary studies. The experimental results demonstrate that the wearable dry electrode prototype, which has a relatively comfortable forehead setup, can efficiently capture vigilance dynamics. The best mean correlation coefficients achieved by our proposed approach are 71.18% and 66.20% in laboratory simulations and real-world driving environments, respectively. The cross-environment experiments are performed to evaluate the simulated-to-real generalization and a best mean correlation coefficient of 53.96% is achieved.

Index Terms—Vigilance estimation, drowsy driving, forehead EOG, eye tracking glasses, dry electrode, wearable device, real-world driving environment.

Manuscript received August 26, 2017; revised January 8, 2018, July 27, 2018, and October 30, 2018; accepted December 14, 2018. Date of publication January 21, 2019; date of current version December 31, 2019. This work was supported in part by the National Key Research and Development Program of China under Grant 2017YFB1002501, in part by the National Natural Science Foundation of China under Grant 61673266, in part by the Technology Research and Development Program of China Railway Corporation under Grant 2016Z003-B, and in part by the Fundamental Research Funds for the Central Universities. The Associate Editor for this paper was Q. Ji. (Corresponding author: Bao-Liang Lu.)

W.-L. Zheng, W. Liu, C. Liu, and B.-L. Lu are with the Key Laboratory of Shanghai Education Commission for Intelligent Interaction and Cognitive Engineering, Center for Brain-Like Computing and Machine Intelligence, Brain Science and Technology Research Center, Department of Computer Science and Engineering, Shanghai Jiao Tong University, Shanghai 200240, China (e-mail: blu@cs.sjtu.edu.cn).

K. Gao, G. Li, J.-Q. Liu, and G. Wang are with the Department of Micro/Nano Electronics, Shanghai Jiao Tong University, Shanghai 200240, China.

Digital Object Identifier 10.1109/TITS.2018.2889962

1524-9050 © 2019 IEEE. Personal use is permitted, but republication/redistribution requires IEEE permission.
See http://www.ieee.org/publications_standards/publications/rights/index.html for more information.

I. INTRODUCTION

VIGILANCE decrement or attention lapse has long been recognized as the critical factor responsible for thousands of deaths and injuries each year in the public traffic community. Driving tasks, particularly truck driving and high-speed trains, require sustained high vigilance. However, efficient techniques for quantifying driver vigilance levels are still lacking, which leads to the inability to provide active feedback for enhancing traffic safety. The National Highway Traffic Safety Administration (NHTSA), an agency of the US Department of Transportation, held a forum called “Asleep at the Wheel: A Nation of Drowsy Drivers” to discuss how to address the problem of drowsy driving [1]. Various questionnaires and performance tasks have been proposed and validated in the literature [2]–[5].

Although considerable progress has been achieved in various areas over the past decades, accurately estimating driver vigilance in real-world driving environments is still difficult. The main reason for this difficulty is that vigilance states are intrinsic mental states that involve temporal evolution rather than a time point. It is difficult to evaluate mental states without using an intrusive stimulus or behavior probe [6]. Traditional techniques for vigilance estimation involve periodically interrupting subjects during the experiments [3]. Moreover, real-world applications require continuous vigilance estimation with high temporal resolution [7]. Vigilance decrement is typically accompanied by both external behaviors, such as head nodding, yawning, and eye closure, and internal physiological changes. Various approaches based on these cues have been developed [8]–[10]. Dong and colleagues presented a review of different driver inattention monitoring systems [11]. Among these various modalities, physiological signals have been found to be relevant for different vigilance levels. However, how to identify reliable and valid biomarkers remains a challenge within the research community [1].

The electroencephalography (EEG) modality is one of the most popular signals used for vigilance estimation because of its advantages of high temporal resolution and noninvasive low-cost properties [12]–[18]. Martel *et al.* [19] observed that increased activity in the alpha frequency range (8-14 Hz) emerged for vigilance decrement and proposed predicting attention lapses in a convert setting up to 10 s in advance. Lin and colleagues integrated lapse monitoring methods and a warning system with a feedback assessment to form a

closed-loop system using EEG power spectra [20]. Different vigilance stages are defined with respect to EEG activities. Posterior alpha oscillations are primarily observed after eye closure, referred to as “idling rhythm” [21]. The phenomenon where the alpha peak frequency exhibits a slight decrease is observed during the transition to drowsiness [22]. All these findings provide fundamental mechanisms and support for EEG-based vigilance estimation.

Although EEG recordings directly measure brain activities, electrooculogram (EOG)-based approaches are easier to implement and ultimately more feasible for large-scale implementations [23] since EOG has a considerably higher signal-to-noise ratio. EOG signals can capture various eye movement parameters, such as blink, saccade, and fixation. Various EOG-based vigilance estimation approaches have been proposed and evaluated in the literature [24]–[28]. Spontaneous eyelid closures (SECs), which refer to periods when the eyelids are closed or almost completely closed with less response to external stimuli, have been found to be an efficient marker for vigilance estimation. Wang *et al.* [6] applied SECs as a nonintrusive vigilance estimation. Damousis and Tzovaras [29] presented a fuzzy fusion method with eyelid activity indicators for accident prediction. Zhang *et al.* [30] proposed measuring cognitive load in a virtual reality-based driving system using multimodal information fusion of eye gaze, EEG, and peripheral physiology data for adolescents with autism spectrum disorder. In our previous study, we demonstrated that EEG and EOG contain complementary information and can be combined to construct a more robust model [31].

A key obstacle to implementing these approaches is how to design long-term, reliable, low-cost, wearable devices for recording bio-signals. The signal quality of the traditional wet electrodes degrades as the electrolyte gel dehydrates over time, and it has a high time cost and is not convenient for setups. Several types of dry flexible electrodes have been proposed due to their low cost, biocompatibility and easy deformation to achieve a desired shape. Polydimethylsiloxane (PDMS) [32]–[34] is a non-conductive silicone-based elastomer, and it has the advantages of flexibility and easy micro-molding for rapid prototyping of microdevices and systems. Carbon nanotubes (CNTs) [35] are an excellent filler for electrically conducting composites because CNTs have a high aspect ratio (length-to-radius ratio), high conductivity and easy percolation at lower concentrations than spherical conductive fillers. With recent advances in flexible dry electrodes and integrated circuit design, mostly driven by sensor networks, the implementation of these sensors appears to be increasingly more promising [36]–[41]. Lin and colleagues developed a wireless and wearable EEG system with five dry electrodes on the frontal areas for evaluating driver vigilance [42], [43]. Mullen *et al.* [44] designed an EEG headset with adjustable tensioning of the flexible dry electrodes contacting the scalp for cognitive monitoring.

The previous designs of dry electrodes were generally fabricated using a conductive polymer [33]–[35] or metal [45], [46]. The conductive polymers are typically not soft enough to adapt to the shrinkage on the surface of

skin, and the conductivity is considerably lower than that of metals [34]. Meanwhile, the metal electrode has a considerably lower impedance than the polymer electrode, but the rigid electrode has the disadvantage of leading to discomfort or even pain [46]. In this study, the textile surface of the conductive fabric enables the electrode to be pasted onto the surface of skin with little clearance. The textile can compensate for the shrinkage on skin and lead to a lower contact impedance. Furthermore, sweat can infiltrate into the conductive fabric and keep the surface of the skin moist, which leads to a reduction in the electrode-skin contact impedance and enables the electrode to record EOG signals similar to wet electrodes.

The majority of these previous studies were performed in laboratory settings [47], [48]. To the best of our knowledge, there are few studies of vigilance estimation that have been performed in real-world driving environments due to various complex challenges that are encountered outdoors. Papadelis *et al.* [24] designed an on-board electrophysiological system for monitoring sleepiness and showed that eye-blinking statistics are sensitive to the driver’s sleepiness. Healey and Picard [49] presented a method for detecting stress using physiological data during real-world driving scenarios. In a recent study Wang *et al.* [50] utilized two electrodes on the placements O1 and O2 to record EEGs of professional bus drivers during an approximately 252 km long driving route. Increasingly more innovative methodologies are being developed to fill research gaps between laboratory settings and real-world environments by using advanced wearable techniques.

In this paper, we design a wearable prototype device that integrates flexible dry electrodes and an acquisition board for recording forehead EOG signals. To capture the vigilance dynamics, we introduce two temporal dependency models, continuous conditional random field and continuous conditional neural field, to construct vigilance estimation models. To evaluate the efficiency of our system, systematic experiments are performed not only in laboratory simulations but also in real-world scenarios under different weather conditions. The dataset (SEED-EOG) used in this study will be freely available to the academic community as a subset of SEED (SJTU Emotion EEG Dataset).¹

II. SYSTEM ARCHITECTURE

Figure 1 shows the flowchart and structure of our proposed system, which includes several parts: flexible dry electrodes, EOG acquisition board, feature extraction for forehead EOG, regression models, and vigilance annotations. The experimental setups for both laboratory simulations and real-world environments are also illustrated in Figure 1.

A. Flexible Dry Electrode

In this study, a novel dry fabric-based electrode was proposed for forehead EOG recording on bare skin. The dry fabric-based electrode was designed to be fabricated using a piece of conductive fabric. The conductive fabric is commonly used to produce protective gear for gravida.

¹<http://bcmi.sjtu.edu.cn/~seed/>

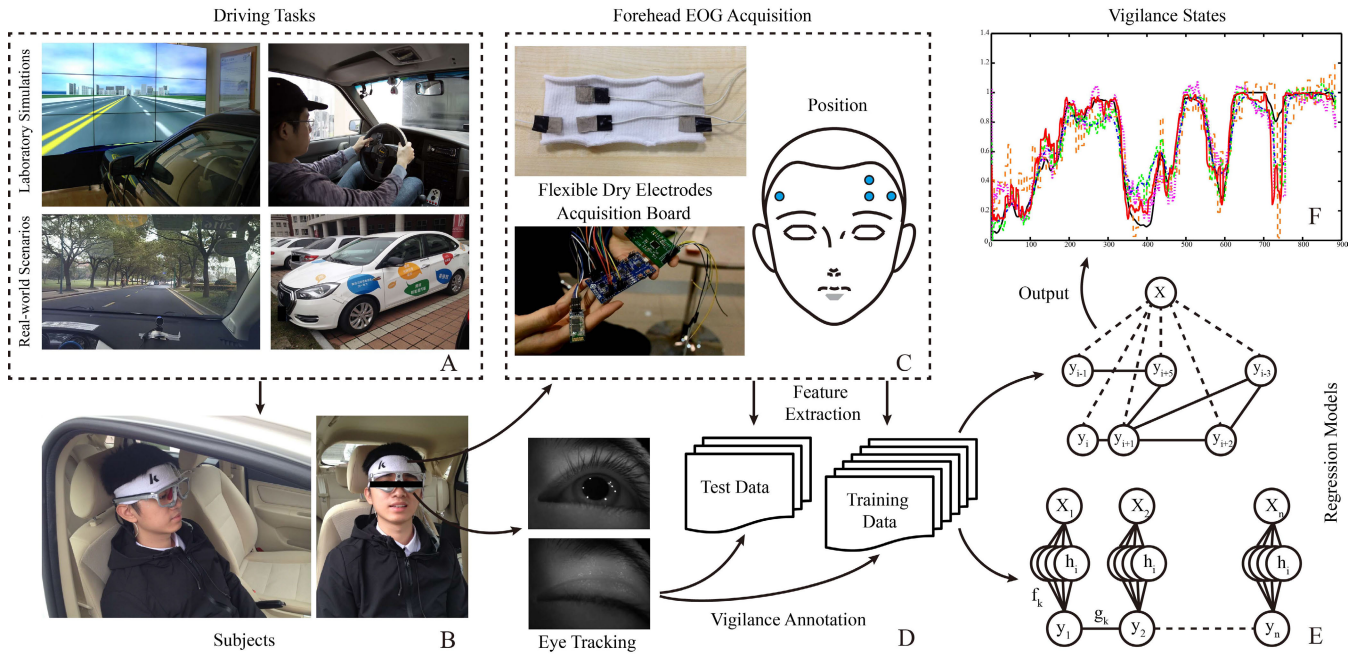


Fig. 1. The flowchart and structure of our proposed system. The subjects are asked to drive a car in the laboratory simulations and to sit in the front passenger seat beside the drivers in the real-world environments (A, B). The simulated driving experiments are performed in a real vehicle without the unnecessary engine. The driving scenes are synchronously updated according to the subjects' operations. The real-world driving experiments are performed under various weather conditions. The forehead EOGs and eye movements are simultaneously recorded using our designed wearable EOG-recording prototype and SMI eye-tracking glasses, respectively (C, D). Regression models using CCRF and CCNF are trained for continuous vigilance estimation (E, F).

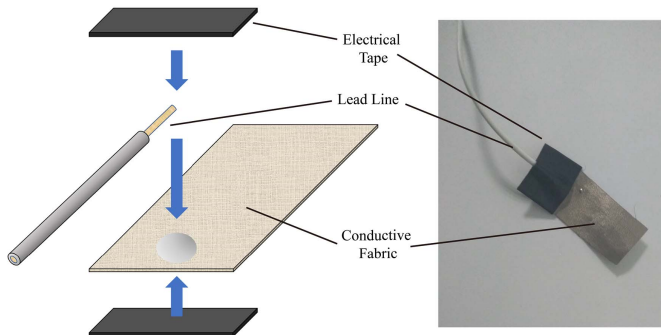


Fig. 2. Design of the dry fabric-based electrode.

Figure 2 shows the design of the dry fabric-based electrode. In contrast to many previous designs of soft dry electrodes produced using conductive polymers or metals, the conductive soft material used in this study is a type of fabric woven using silver-coated nylon line. Conductive fabric has a considerably higher impedance conductivity rate (conductivity of approximately 0.07 Ohm/square, similar to that of metals) than conductive polymer materials, and moreover, it can be substantially softer than rubber-based conductive polymer materials or metal-based materials.

To fabricate the electrode used in this study, the fabric was cut into pieces that were 17 mm long and 10 mm wide. The conductive fabric pieces were then pasted onto the surfaces of wet wipes. The lead lines were then welded onto the conductive fabric pieces. During welding, the wet wipes can prevent the conductive fabric from burnout. After welding, the contact

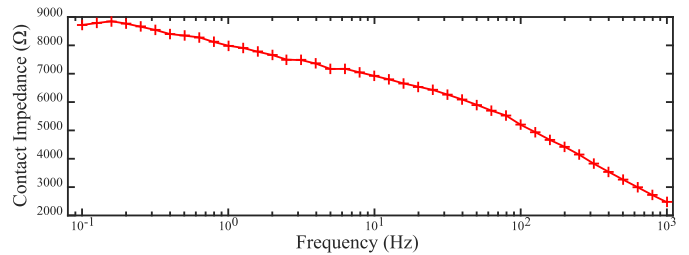


Fig. 3. Contact impedance of dry conductive fabric electrodes on forehead.

of the conductive fabric and lead line was reinforced using electrical tape. The connections between the lead wire and the conductive fabric can be processed into metal button shapes for long-term usage. In this way, the connections are strong enough and feasible for electrode replacement.

To evaluate the performance of the conductive fabric electrodes, the contact impedance of the dry conductive fabric electrode was measured using an electrochemical workstation (660C, Chiinstru-ments Ltd., China). Figure 3 shows the contact impedance at different frequencies. Due to the infiltration of sweat and the larger contact square than traditional wet electrodes, the contact impedance of the dry conductive fabric electrodes is similar to that of wet electrodes [51]–[54].

We performed experiments for measuring forehead EEG alpha rhythm to evaluate the performance of the dry conductive fabric electrodes. The alpha rhythm of EEG components is dominant during eye closure period [24], [31], which is an efficient approach to evaluating the quality of EEG data. Figure 4(a) shows the forehead EEG signals recorded on

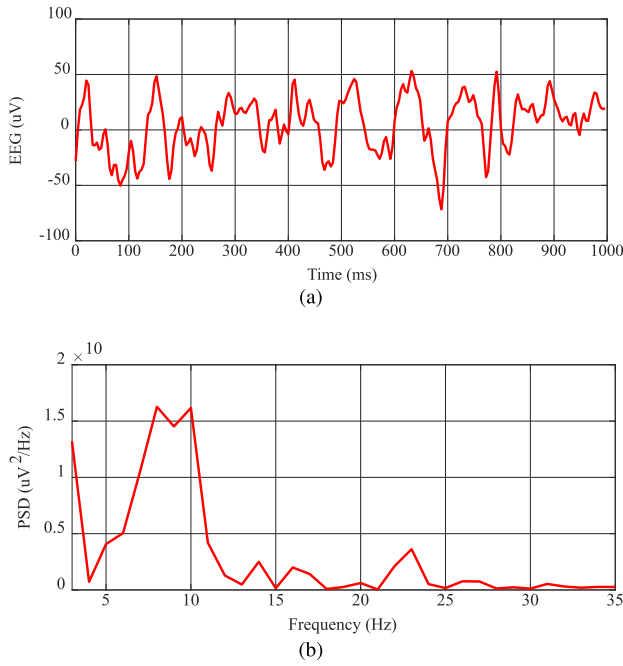


Fig. 4. EEG signals recorded on the site *FP1* during an eye closure period with the dry conductive fabric electrodes: (a) EEG signals recorded with eyes closed and (b) PSD of the recorded EEG signals.

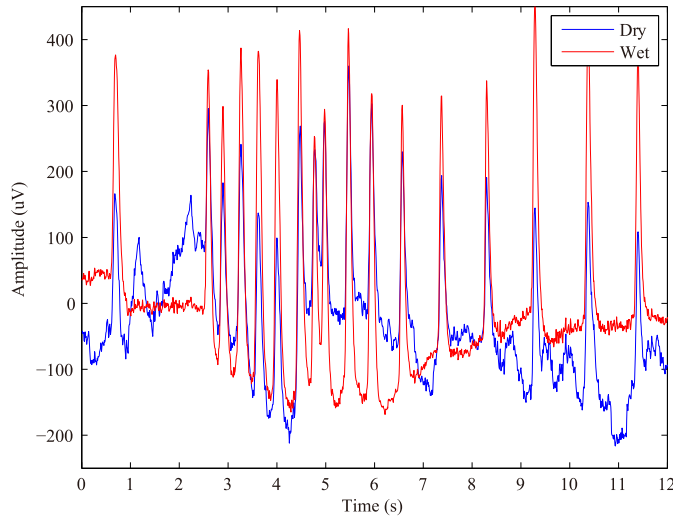


Fig. 5. The raw signals recorded simultaneously with the commercial wet electrode (red) and the dry fabric electrode (blue) on the forehead site *FP1*.

the site *FP1* during an eye closure period using the dry fabric electrodes, and Figure 4(b) shows its corresponding power spectral density. A peak corresponding to alpha rhythm can be observed between 8 and 11 Hz in Figure 4(b). The results of the alpha rhythm test demonstrate and verify that the electrodes can even be used for recording EEG signals, which guarantees the quality of the forehead EOGs recorded in this study.

Because EOGs have much higher signal-to-noise ratio in comparison with EEGs, EOG signals can be well recorded by the designed dry electrodes. Figure 5 shows the raw signals recorded simultaneously by using the dry fabric electrode

TABLE I
SUMMARY OF MAIN COMPONENTS AND TECHNICAL PARAMETERS OF THE PROPOSED FOREHEAD EOG ACQUISITION SYSTEM

Sub-system	Component	Parameter
EOG	Sensors	Ag/AgCl
	Sampling rate	250 Hz
	Bandpass Filter	4-30 Hz
	Gain	12X
	Montage	Frontal unipolar four-channel
	Frontal End	ADS1298 (built-in 24-bit ADC)
Bluetooth	MCU	Nordic nRF51822
	Protocol	Bluetooth EDR
Terminals	Baud-rate	57600 bps
	Operating System	Android 4.0+
	Processor	1.2 GHz+

and the commercial wet electrode on the site *FP1* with the Neuroscan recording system. We can see that the quality of the dry electrode is comparable with that of wet electrode. Although there are more noises and fluctuations in signals recorded by the dry fabric electrode, the signals can well capture the characteristic waves of eye movements, e.g., blink and saccade.

B. EOG Acquisition Board

The EOG acquisition board was a custom board designed by our group, as shown in Figure 6, and it incorporated one TI ADS1298 analog front end for recording EOGs, a Nordic nRF51822 microcontroller and a Bluetooth module (BC6140, classical Bluetooth) for wireless transmission of the data to a PC or any mobile device. A gain of 12 was used on the ADS1298 differential amplifiers. The built-in 24-bit ADC had a resolution of approximately 0.4 uV. The board was battery powered, and the battery can be recharged using a micro-USB interface. Our acquisition board was capable of simultaneously recording 8-channel EOG signals (4 channels are used in this study, as shown in Figure 1C) and was approximately 4.5 × 6.5 cm in size. The sampling frequency was set to 250 Hz.

To measure the electrode-scalp impedance for each individual electrode, we used the “lead-off” detection feature of the TI ADS1298. A 24 nA sinusoidal AC current at a known frequency of 30.5 Hz was injected for each electrode (more details about this AC lead-off detection technique can be found in [55]). If any electrode was detected as having lead-off status, a blue LED on the board would illuminate. In this way, a low-impedance conductive path between drivers and our acquisition board can be guaranteed, and accurate measurement of the EOG signals can be achieved.

The developed EOG acquisition board contained four sewing holes around the board, which allowed the entire board to be sewn onto a light-weight elastic headband for real-life applications. The entire prototype and system diagram are shown in Figures 6 and 7, respectively. More technical details are summarized in Table I.

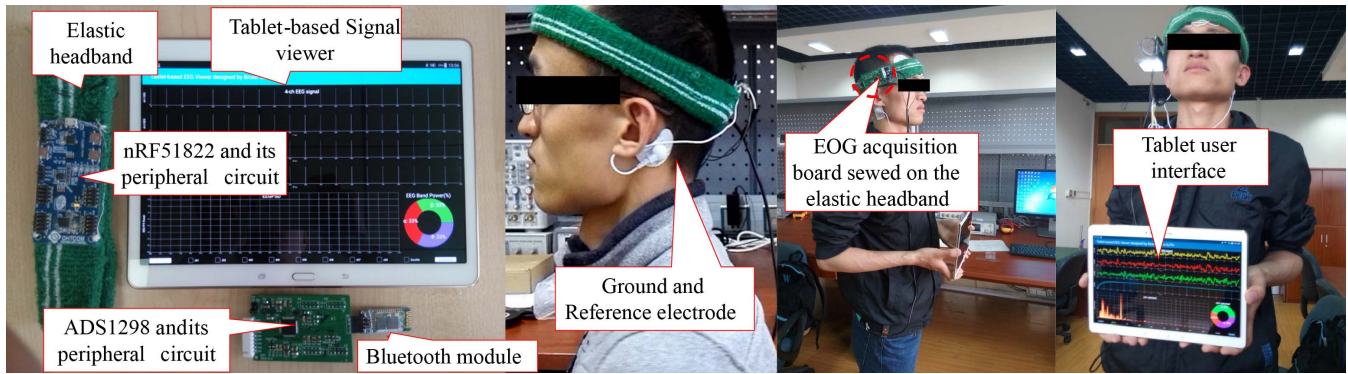


Fig. 6. The EOG acquisition board designed by our group and its paired tablet user interface.

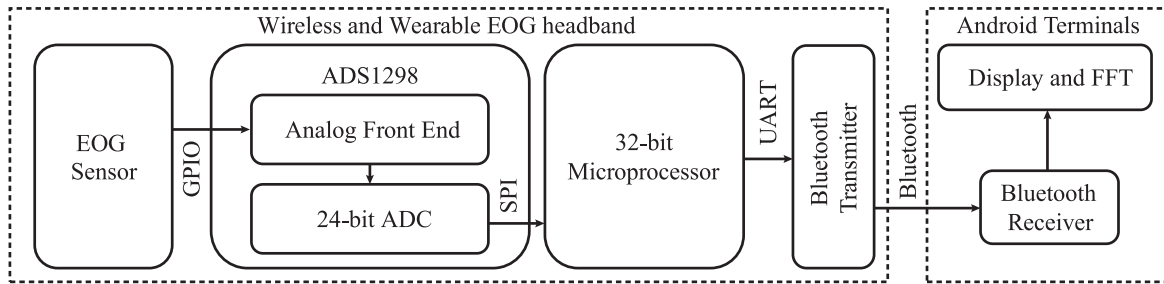


Fig. 7. System diagram and signal flow of the designed EOG acquisition board.

C. Feature Extraction for Forehead EOG

Compared with the conventional EOG setups, which mount the electrodes around the eyes, we proposed placing all the electrodes on the forehead, as shown in Figure 1C, in our previous studies [28], [31], [56]. This design has been demonstrated to reduce discomfort in real-world applications and to be efficient for wearable vigilance estimation. The signals of the vertical two electrodes are used for extracting vertical EOG (VEO) using independent component analysis (ICA) [57], whereas those of the horizontal two electrodes are subtracted for extracting horizontal EOG (HEO). Detailed comparisons of conventional EOG and forehead EOG can be found in [31]. After preprocessing the raw forehead signals, VEO and HEO were obtained for extracting the details of eye movements, such as blink, saccade, and fixation.

To detect blinks and saccades, the wavelet transform method was used since it is sensitive to singularities. We computed the continuous wavelet coefficients at a scale of 8 using a Mexican hat wavelet defined by

$$\psi(t) = \frac{2}{\sqrt{3\sigma\pi^{\frac{1}{4}}}} \left(1 - \frac{t^2}{\sigma^2}\right) e^{-\frac{t^2}{2\sigma^2}}, \quad (1)$$

where σ is the standard deviation. The peak detection algorithm on the wavelet coefficients was used to detect blinks and saccades from the forehead VEO and HEO, respectively.

We applied thresholds on the continuous wavelet coefficients of the forehead VEO and HEO to detect positive and negative peaks and encode them into sequences. For this purpose, a positive peak was encoded as '1', and a negative peak was encoded as '0'. In continuous wavelet coefficients,

positive and negative peaks denote that there are high amplitude changes in the raw signals. If the amplitude increases, there are two successive negative and positive peaks '01' and if the value decreases, two successive positive and negative peaks '10' are observed. A saccade (amplitude increases or decreases in HEO) is characterized by a sequence of two successive positive and negative peaks in the coefficients. A blink (amplitude increases and then decreases in VEO) contains three successive large peaks, namely, negative, positive, and negative, and the time between two negative peaks should be smaller than the minimum time. Therefore, segments with '01' or '10' were recognized as saccade candidates, and segments with '010' were recognized as blink candidates.

Moreover, there are some other constraints, such as slope, correlation, and maximal segment length, for guaranteeing a precise detection of blinks and saccades. After detecting blinks and saccades, we computed the statistical parameters, such as the mean, maximum, variance, and derivative of different eye movements with an 8 s non-overlapping window as the forehead EOG features. We extracted a total of 36 forehead EOG features from the detected blinks, saccades, and fixations, as shown in Table II. For more details regarding the extraction of forehead EOG features, please refer to our previous study [31].

D. Regression Models

Vigilance states are the human intrinsic mental states that involve temporal evolutions. Therefore, the samples of previous and current states have meaningful relations, and these interactions should not be discarded. Conventional regression

TABLE II
THE DETAILS OF THE EXTRACTED 36 EOG FEATURES

Group	Extracted Features
Blink	maximum/mean/sum of blink rate
	maximum/minimum/mean of blink amplitude, mean/maximum of blink rate variance and amplitude variance
	power/mean power of blink amplitude
	blink numbers
	maximum/minimum/mean of saccade rate and saccade amplitude, maximum/mean of saccade rate variance and amplitude variance, power/mean power of saccade amplitude, saccade numbers
Saccade	mean/maximum of blink duration
	variance and saccade duration variance
Fixation	maximum/minimum/mean of blink duration and saccade duration.

models such as support vector regression (SVR) do not explicitly model the temporal dependency. In this paper, we applied two temporal dependency models, namely, continuous conditional neural field (CCNF) and continuous conditional random field (CCRF), to capture the vigilance dynamics [31] and compared their performance with those of the conventional SVR model and the dynamic model using the Linear Dynamic System (LDS) algorithm.

CCNF and CCRF are extensions of conditional random field (CRF) [58] for continuous variable modeling. These models can incorporate temporal or spatial information and have shown promising performance in various applications [59], [60]. CCNF combines the nonlinearity of conditional neural fields [61] and the continuous output of CCRF. Compared with CCRF, CCNF can have multi-dimensional features as inputs.

The probability distribution of CCNF for a particular sequence is defined as follows:

$$P(\mathbf{y}|\mathbf{x}) = \frac{\exp(\Psi)}{\int_{-\infty}^{\infty} \exp(\Psi) d\mathbf{y}}, \quad (2)$$

where $\int_{-\infty}^{\infty} \exp(\Psi) d\mathbf{y}$ is the normalization function, $\mathbf{x} = \{x_1, x_2, \dots, x_n\}$ is a set of input observations, $\mathbf{y} = \{y_1, y_2, \dots, y_n\}$ is a set of output variables, and n is the length of the sequence.

There are two types of features defined in these models: vertex features f_k and edge features g_k . The potential function Ψ is defined as follows:

$$\Psi = \sum_i \sum_{k=1}^{K_1} \alpha_k f_k(y_i, \mathbf{x}_i, \boldsymbol{\theta}_k) + \sum_{i,j} \sum_{k=1}^{K_2} \beta_k g_k(y_i, y_j), \quad (3)$$

where $\alpha_k > 0$, $\beta_k > 0$, the vertex features f_k denote the mapping from \mathbf{x}_i to y_i with a one-layer neural network, and $\boldsymbol{\theta}_k$ is the weight vector for the neuron k .

The vertex features of CCNF are defined as

$$f_k(y_i, \mathbf{x}_i, \boldsymbol{\theta}_k) = -(y_i - h(\boldsymbol{\theta}_k, \mathbf{x}_i))^2, \text{ and} \quad (4)$$

$$h(\boldsymbol{\theta}, \mathbf{x}_i) = \frac{1}{1 + e^{-\boldsymbol{\theta}^T \mathbf{x}_i}}, \quad (5)$$

where the optimal number of vertex features K_1 is tuned through cross-validation. In our experiments, we evaluated $K_1 = \{10, 20, 30\}$.

The edge features g_k denote the similarities between observations y_i and y_j , which are defined as

$$g_k(y_i, y_j) = -\frac{1}{2} S_{i,j}^{(k)} (y_i - y_j)^2, \quad (6)$$

where the similarity measure $S^{(k)}$ controls the existence of the connections between two vertices.

In the experiments, K_2 was set to 1, and $S^{(k)}$ was set to 1 when two nodes i and j are neighbors; otherwise, $S^{(k)}$ was 0. The formulas for CCRF are the same as those for CCNF, except for the definition of vertex features. The vertex features of CCRF are defined as

$$f_k(y_i, \mathbf{x}_{i,k}) = -(y_i - \mathbf{x}_{i,k})^2. \quad (7)$$

The training of parameters in CCRF and CCNF is based on the conditional log-likelihood $P(\mathbf{y}|\mathbf{x})$ as a multivariate Gaussian. For more details regarding the learning and inference of CCRF and CCNF, please refer to [60]. The outputs of support vector regression are used to train CCRF, and the original multi-dimensional features are used to train CCNF.

E. Vigilance Annotation

The key challenge in vigilance estimation is how to automatically label the recorded data, provided that a supervised machine learning framework is used. This challenge is extremely difficult because the ground truth of the intrinsic vigilance states cannot be obtained directly, particularly in real-world scenarios. Various vigilance annotation methods have been proposed in the literature, such as lane departure [43] and local error rates [16]. However, these methods involve an intrusive stimulus or behavioral probe, which periodically interrupts subjects and disrupts the spontaneous vigilance fluctuation that we aim to observe [6]. Moreover, these methods are not appropriate for real-world driving tasks considering safety issues since they contain dual tasks that introduce distractions. Therefore, an efficient nonintrusive cognitive monitoring approach is attractive for our objectives.

Spontaneous eyelid closures (SECs) have been found to be an efficient proxy for vigilance state. Based on SECs, PERCLOS, which refers to the percentage of eye closure, is one of the popular vigilance indices used in various studies [11], [62], [63]. However, traditional approaches utilize facial videos to detect eye states and calculate the scores, which are dramatically degraded with changing illumination and heavy occlusions. In our previous study [31], [64], we proposed an alternative approach to vigilance annotation by using eye-tracking glasses. Calculating the PERCLOS index for vigilance annotation from eye-tracking glasses permits nonintrusive cognitive monitoring, which is feasible for both the simulated and real driving environments that we focus on in this study.

Through eye-tracking glasses, we can obtain accurate eye movement parameters, such as blink, saccade, and fixation. The captured pupil images are shown in Figure 1D. The eye-tracking-based PERCLOS index can be calculated from the

percentage of the durations of blinks and ‘CLOS’ over a specified time interval as follows:

$$PERCLOS = \frac{blink + CLOS}{interval}, \text{ and} \quad (8)$$

$$interval = blink + fixation + saccade + CLOS, \quad (9)$$

where ‘CLOS’ denotes the duration of the eye closures. This approach allows vigilance annotation to be conducted in a very natural way without excessive interference. Therefore, we can observe the vigilance fluctuation of subjects without interruptions.

III. EXPERIMENTAL SETUP

A. Laboratory Driving Simulations

We developed a simulated driving system in the laboratory, which included a large LCD screen showing highway scenes. The simulated driving environment was programmed with OGRE3D graphics rendering engine and OpenAL 3D audio API. The scenarios include a four-lane highway, various cars, buses, traffic signs, buildings, and tunnels. The subjects were asked to sit inside a real vehicle without the engine and drive the vehicle in the simulated environment shown on the front screen. The subjects could control the vehicle in the virtual driving environment using a Logitech steering wheel controller that consists of a steering wheel and a gas pedal. The scenes were simultaneously updated as feedback to enhance the engagement and reality. The simulated driving scenes are shown in Figure 1A.

There were a total of twenty subjects (mean age: 22.6, STD: 2.52, 2 females) that participated in our laboratory simulated driving experiments. Among these subjects, fourteen subjects (mean age: 21.5, STD: 1.0, 1 female) only participated in the simulated driving experiments and the other six subjects participated in both the simulated and real-world driving experiments for comparisons. All of the subjects had normal or corrected-to-normal vision. Caffeine, tobacco, and alcohol were prohibited prior to participating in the experiments. To ensure that all subjects could proficiently perform the experiments, a preliminary test was performed at the beginning of the experiments.

To collect the data of low vigilance states, we designed two setups for the experiments. The road in the simulation software is primarily straight and monotonous to more easily induce fatigue in the subjects. The experiments were performed in the early afternoon (approximately 13:30) after lunch and at nightfall (approximately 19:00) after dinner according to the circadian rhythm of sleepiness [65]. The duration of the entire experiment was approximately 2 hours.

The forehead EOG signals were recorded using the wearable dry prototype device while the subjects participated in the experiments. Eye movements were simultaneously recorded using SMI ETG eye-tracking glasses,² and the facial video was recorded by a camera mounted in front of the subjects.

²<http://eyetracking-glasses.com/>

B. Real-World Driving Experiments

Ten healthy subjects (mean age: 24.2, STD: 2.7, 1 female) participated in the real-world driving experiments. In order to compare the simulated and real-world driving experiments, six of the ten subjects also participated in the laboratory driving simulations. To ensure safety when the subjects were drowsy, the subjects were asked to sit in the front passenger seat beside the drivers during the experiments. The driving route was inside Shanghai Jiao Tong University, Minhang Campus, in Shanghai, China. The route was planned to take subjects through situations where different vigilance levels were likely to occur. The route contained crowded areas with many pedestrians and sparse areas with monotonous stretches. At the beginning of the experiment, both drivers and subjects were shown a map of the driving route to keep the drives consistent. Instructions explaining the complete experimental procedure were given to each subject. The experiments were performed in electric vehicles. One lap of the route was approximately 5.5 km. The driving speed limit was kept at approximately 30 km/h, and the duration of the driving was approximately 1.5 hours with several laps.

When driving on the road, the forehead EOGs, eye movements, and facial videos were simultaneously recorded. During the experiments, an observer accompanied the drivers in the car to monitor the signal recording. The observer sat in the rear seat behind the subjects to avoid interfering with the drivers and the subjects. All of the experiments were performed in the early afternoon (approximately 13:30) after lunch and at nightfall (approximately 19:00) after dinner, similar to the laboratory simulated experiments. Figure 8 shows the sample frames recorded from the scene camera.

The real-world driving experiments were performed under various illumination and weather conditions, including sunny, cloudy, windy, rainy and night time. The weather and illumination conditions of the ten experiments were rainy, windy, cloudy, rainy, sunny, sunny, cloudy, cloudy, sunny, and night time, respectively. As shown, for some extreme conditions, it is very difficult to detect vigilance levels from facial videos for traditional image-based methods due to the severe illumination changes [11]. Conversely, the quality of EOG is not sensitive to these factors. Note that this is a very important advantage of the EOG-based vigilance estimation approach over the traditional facial video-based methods.

C. Evaluation Details

For the continuous regression problems, we used the root mean square error (RMSE) and correlation coefficient (COR) as the evaluation metrics. RMSE is the squared error between the prediction and the ground truth, and it is defined as follows:

$$RMSE(Y, \hat{Y}) = \sqrt{\frac{1}{N} \sum_{i=1}^N (y_i - \hat{y}_i)^2}, \quad (10)$$

where $Y = (y_1, y_2, \dots, y_N)^T$ is the ground truth and $\hat{Y} = (\hat{y}_1, \hat{y}_2, \dots, \hat{y}_N)^T$ is the prediction. COR provides an evaluation of the linear relationship between the prediction

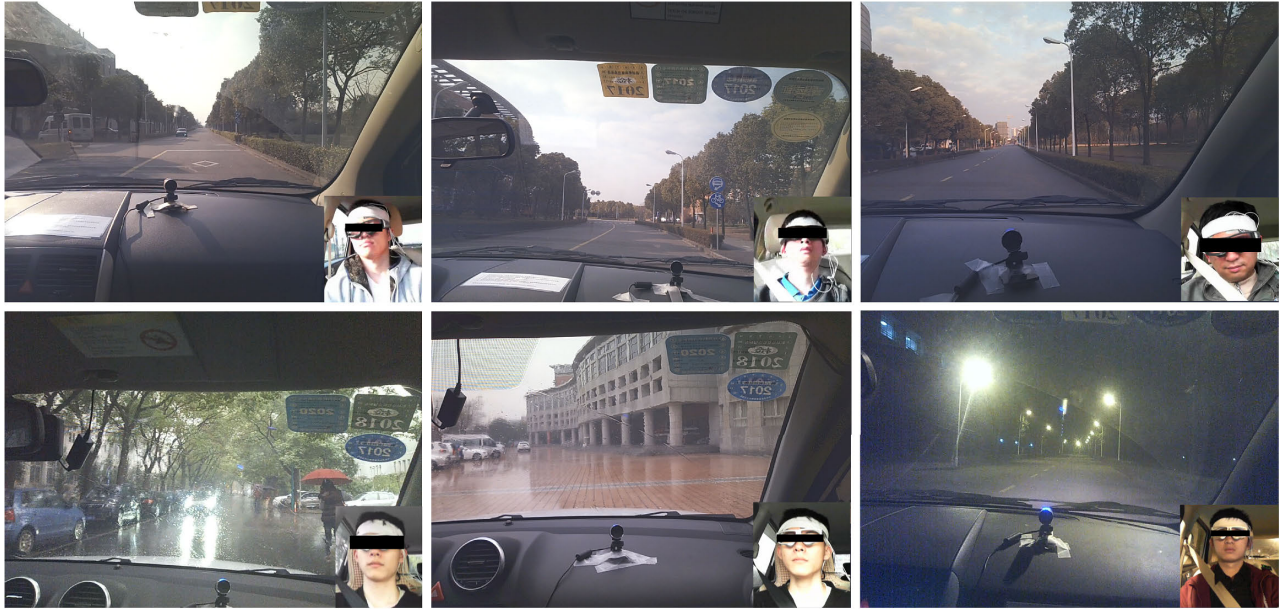


Fig. 8. The sample frames recorded from the scene camera of eye-tracking glasses as the first perspective. The real-world driving experiments were performed under various illumination and weather conditions, including sunny, cloudy, windy, rainy and night time.

and the ground truth, which reflects the consistency of their trends. Pearson's correlation coefficient is defined as follows:

$$COR(Y, \hat{Y}) = \frac{\sum_{i=1}^N (y_i - \bar{y})(\hat{y}_i - \bar{\hat{y}})}{\sqrt{\sum_{i=1}^N (y_i - \bar{y})^2 \sum_{i=1}^N (\hat{y}_i - \bar{\hat{y}})^2}}, \quad (11)$$

where \bar{y} and $\bar{\hat{y}}$ are the means of Y and \hat{Y} , respectively.

There are about 885 and 675 samples for each simulated and real driving experiments, respectively. For evaluation, we split the entire data from one experiment into five successive sessions and performed 5-fold cross validation. We concatenated the predictions and ground truth of the five sessions and calculated the RMSE and COR as the evaluation metrics. In general, the more accurate the model is, the higher the COR is and the lower the RMSE is.

For parameter tuning of the regression models, we utilized support vector regression (SVR) with radial basis function (RBF) kernel as a basic regression model. The optimal values of the parameters c and g were tuned using grid search. The CCRF and CCNF regularization hyper-parameters for α_k and β_k were chosen based on a grid search in $10^{[0,1,2]}$ and $10^{[-3,-2,-1,0]}$ using the training set, respectively.

In order to compare the performance of the temporal dependency models, CCRF and CCNF, with other dynamic models, linear dynamic system (LDS) [66], [67] approach is adopted with the outputs of SVR as inputs (called SVR-LDS). LDS aims to find the mapping between observed variables and hidden variables. And the parameters can be optimized using the Expectation Maximization (EM) algorithm based on the observed variables.

IV. EXPERIMENTAL RESULTS

A. Laboratory Driving Simulations

In this section, we present the experimental results of the simulated driving experiments in the laboratory. First, we

evaluated the performances of CCRF and CCNF with varying sequence length n . The sequence length determines the strength of modeling temporal dependency. A longer sequence length makes inference based on larger time windows with large-scale information. However, it might reduce the representational capacity for the vigilance fluctuations. There is a trade-off between exploration and exploitation.

Figure 9 shows the performances of CCRF and CCNF with varying sequence length n for the first 14 subjects. From the experimental results, the performance of CCRF is relatively stable, while that of CCNF is slightly degraded with a larger sequence length. The best sequence lengths of CCRF and CCNF are nine and four, where CCRF and CCNF achieve the best mean performance of 0.7104 ± 0.1491 and 0.7118 ± 0.1134 for COR, respectively, and their mean RMSEs are 0.1515 ± 0.0552 and 0.1523 ± 0.0604 , respectively. We observe that although the predictions of CCNF obtain higher correlation with the ground truth, they have larger mean square errors than those of CCRF. Moreover, we find that if vigilance estimation with high temporal resolution in some situations is vital, CCRF and CCNF with a much smaller sequence length (2) can achieve slightly lower performances of $0.6770/0.6943$ and $0.1632/0.1576$ for COR and RMSE, respectively.

Figure 10 shows the detailed performances of different models for the twenty individual subjects. The mean COR values of the baseline method SVR, SVR-LDS, CCRF, and CCNF are 0.6679 ± 0.1717 , 0.6776 ± 0.1718 , 0.7179 ± 0.1588 , and 0.7215 ± 0.1596 , respectively and the corresponding mean RMSE values are 0.1845 ± 0.0762 , 0.1806 ± 0.0746 , 0.1647 ± 0.0684 , and 0.1619 ± 0.0787 , respectively. The performance of SVR-LDS is lightly better than SVR. The temporal dependency models (CCRF and CCNF) perform better than the conventional methods of SVR and SVR-LDS in terms of the mean COR and RMSE. These results indicate that incorporating temporal dependency information into

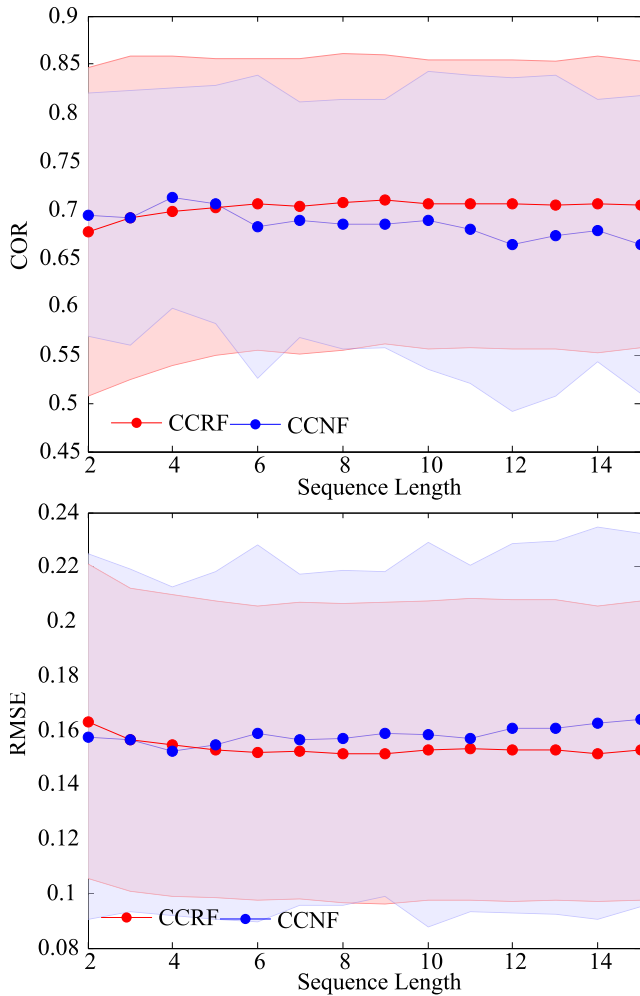


Fig. 9. The performances of CCRF and CCNF with varying sequence length in the simulated driving experiments.

vigilance estimation is efficient. These findings are consistent with previous studies of modeling temporal and spatial dependencies when analyzing time series data in the literature [59]–[61], [68].

To verify whether the predictions from our proposed approaches are consistent with the subjects' true behaviors and cognitive states, the continuous vigilance estimation of one experiment (Subject 6) is shown in Figure 11. The snapshots in Figure 11 show the eye states corresponding to different vigilance levels, which are captured using eye-tracking glasses. We can observe that our proposed system that combines the wearable dry EOG prototype and the temporal dependency models can moderately predict the continuous vigilance levels and their trends.

B. Real-World Driving Experiments

In this section, we extend the evaluations of our designed vigilance estimation system to the real-world driving tasks. Figure 12 shows the performances of CCRF and CCNF with varying sequence length n . As shown, in the real scenarios, CCNF performs better than CCRF with a higher COR and

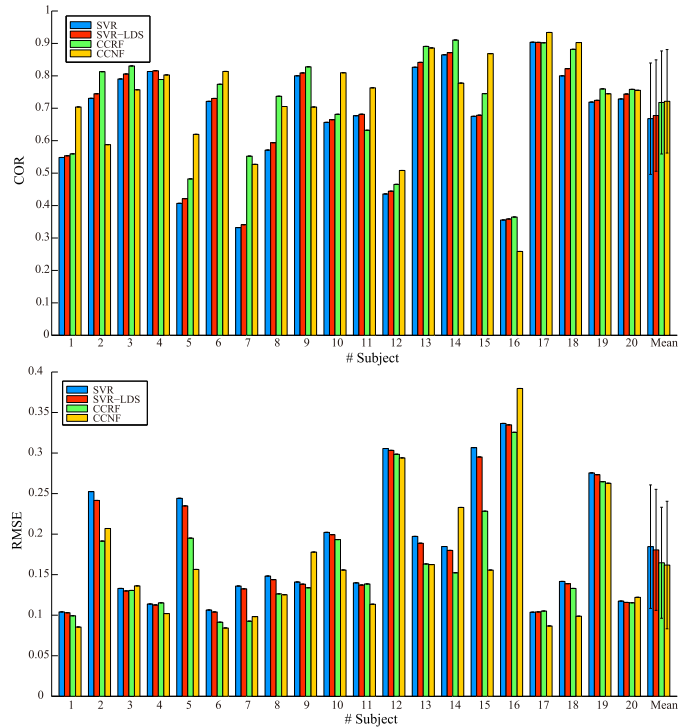


Fig. 10. The detailed performances of different models: SVR, SVR-LDS, CCRF, and CCNF for individual subjects in the simulated driving experiments. The last six subjects are corresponding to Subjects 1, 3, 5, 6, 7, and 9 in the real-world driving experiments.

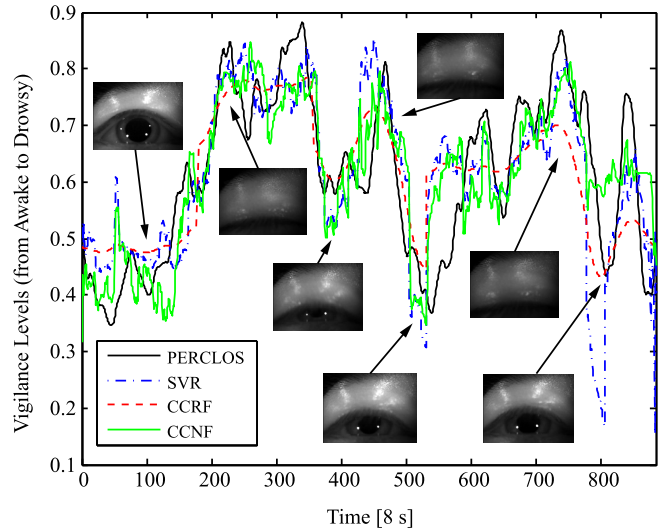


Fig. 11. The continuous vigilance estimation of different methods in one experiment (Subject 6) in the simulated driving experiments. As shown, the predictions from our proposed system are almost consistent with the true subjects' vigilance states.

lower RMSE. The sequence length n does not considerably influence their performances. CCRF and CCNF achieve their peak performances with sequence lengths of 7 and 9, respectively. We compare the performances of different models individually in Figure 13. The mean CORs of SVR, SVR-LDS, CCRF, and CCNF are 0.5784 ± 0.1882 , 0.5870 ± 0.1855 , 0.6133 ± 0.1779 , and 0.6620 ± 0.2688 , respectively, while

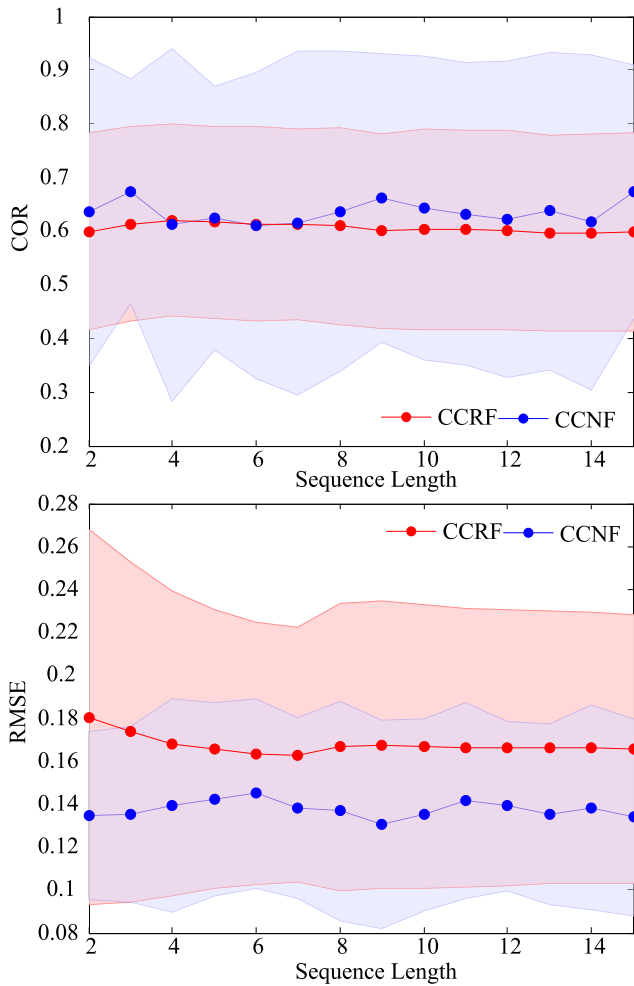


Fig. 12. The performances of CCRF and CCNF with varying sequence length in the real-world driving experiments.

their mean RMSEs are 0.1890 ± 0.0953 , 0.1858 ± 0.0933 , 0.1630 ± 0.0594 , and 0.1307 ± 0.0486 , respectively. The conclusion that the temporal dependency models perform better than the baseline method SVR is validated in the real-world tasks. Figure 14 presents the predictions of different models and the ground truth of vigilance fluctuations.

Compared with the performance of the laboratory simulated driving, the performance of our system in real-world driving environments decreases approximately 0.0498 for COR and 0.0216 for RMSE. Considering the challenges of complex outdoor environments, including extreme weather such as rainy and cloudy conditions, our wearable system can still perform well with slightly decreased performance. These results demonstrate that our proposed vigilance estimation system with wearable dry forehead EOG and temporal dependency models is efficient in both simulated and real-world driving environments.

In order to compare the performance between different environments, Six of the ten subjects (Subjects 1, 3, 5, 6, 7, and 9) in the real-world driving experiments also participated in the laboratory driving experiments. Table III shows the performance comparison of the same subjects in different scenarios.

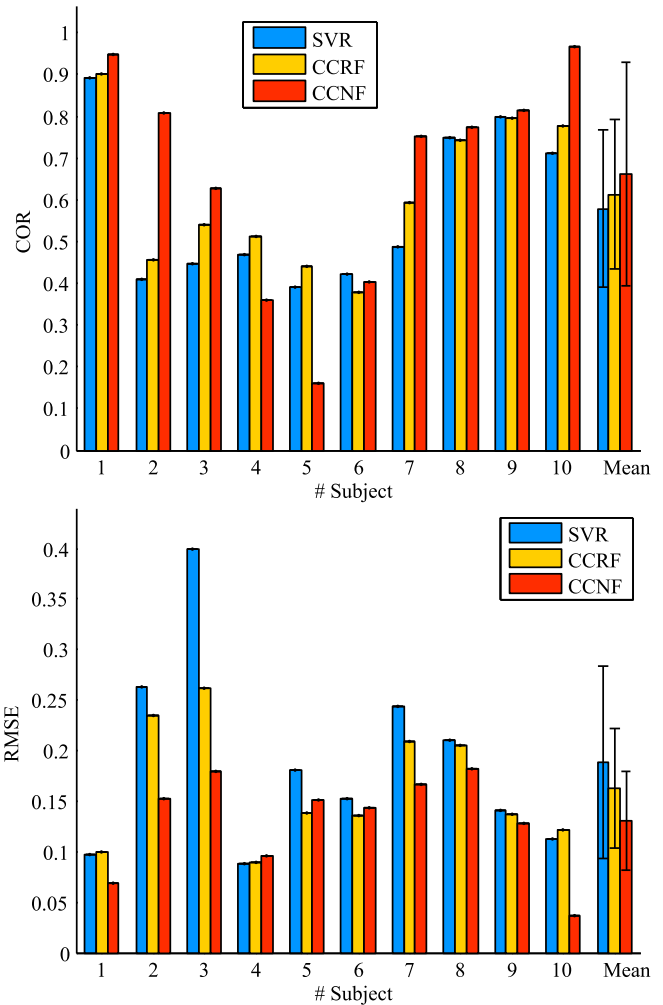


Fig. 13. The detailed performances of different models, SVR, CCRF, and CCNF, for individual subjects in the real-world driving experiments.

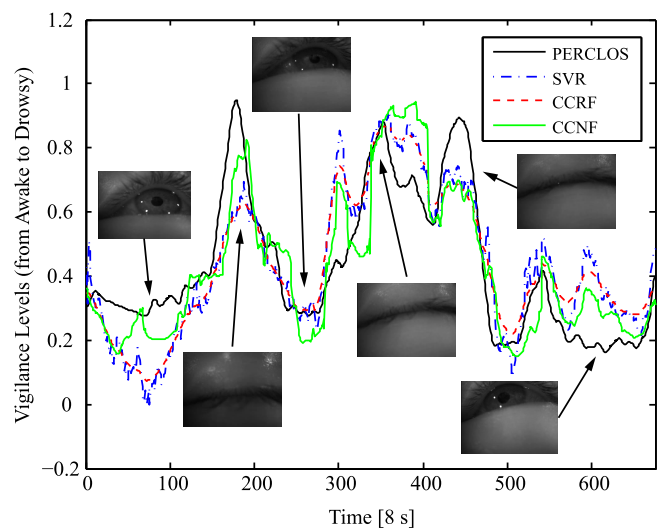


Fig. 14. The continuous vigilance estimation of different methods in one experiment (Subject 9) in the real-world driving experiments.

Similarly, the temporal dependency models CCRF and CCNF achieve better performance than the baseline approaches. In terms of the mean COR evaluations, the performance

of our system are better in simulated driving environments with an improvement of about 0.12. But there are also some exceptions, e.g., Subjects 1, 3, and 9 obtain better results in the real-world driving experiments. Moreover, the mean RMSEs are larger (about 0.04) in the simulated experiments, although some subjects (e.g., Subjects 5, 6, and 9) have different results. The RMSE of Subject 3 is much larger than those of the others in the simulated driving experiments, which highly degrades the overall performance. It is difficult to compare the performance of the system between each pair of experiments, even for the same subjects. Because there are many environment factors that can highly influence the prediction performance. In general, the performance in the controlled laboratory simulated scenarios is better than that in the real-world environments.

C. Cross-Environment Experiments: From Simulated to Real-World Scenarios

Compared with the real-world scenarios, it is much easier to collect and annotate the data in the controlled laboratory simulations. An intuitive and straightforward approach is to train models on the simulated data and make inference on the data in the real-world applications. In this Section, we will perform the cross-environment experiments and evaluate the simulated-to-real generalization of our system. The labeled data in the simulated driving experiments are used as the training data and the performance of different models are evaluated on the data of the real-world driving experiments.

The experimental results of cross-environment experiments are shown in Table IV. The best mean COR and RMSE are achieved using CCNF with the values of 0.5396 and 0.2262, respectively. In comparison with the results (COR with 0.6620 and RMSE with 0.1307) in the real-world driving experiments, our proposed system have a degraded performance of 0.1224 for COR and 0.0955 for RMSE. Even with the large variations between the simulated and real-world environments, the system can still detect the vigilance dynamics moderately in the real-world driving task with a limited number of labeled data in the simulated environment for training.

There exist many discrepancies between simulations and the real world, which make knowledge transfer from simulations to real-world applications challenging. These discrepancies called the reality gap form the barrier to using the simulated data on models training in the real world. These factors cause significant differences between the data distributions of the simulations and the real world, which dramatically degrade the prediction performance. It is difficult to develop robust systems in real-world applications with only simulation data. Various approaches have been proposed to bridge the reality gap, e.g., domain adaptation [69] and domain randomization [70].

V. DISCUSSION

In our previous study [31], we constructed vigilance estimation models with forehead EOGs recorded with the traditional wet electrodes using a commercial Neuroscan system, which represents the gold standard. The mean COR

and RMSE of our previous wet-electrode-based approach are 0.7773 ± 0.1745 and 0.1188 ± 0.0391 , respectively. Compared with our previous study, we design a wearable dry EOG prototype that is feasible for real-world scenarios with a moderate decrease in prediction performance to some extent.

Although considerable progress in vigilance estimation has been achieved over the past decades, few studies have been performed in real-world scenarios [24], [49], [50], and most studies are performed in controlled laboratory environments. A small number of studies in real-world environments are mostly based on facial videos due to easy setups at the cost of degraded performance. There is a large gap between simulations and real conditions. In this study, we perform both simulated and real-world experiments for our designed system to fill this gap. The experimental results demonstrate the efficiency of our system in real-world applications.

Considering safety issues, we actually analyze the data of subjects sitting in the front passenger seat rather than drivers in real driving environments. Since the operations are different for drivers and passengers, the performance of the system for real drivers requires further investigation. Note that although we have evaluated the performance of our system in real-world driving environments, the real-time online performance has not been tested, which should be evaluated in the near future.

One of the limitations for constructing robust vigilance estimation models is the high cost of collecting a large amount of physiological data. By leveraging the feasibility and wearability of our vigilance estimation prototype, we are able to collect a large amount of related data, and these large datasets can actively help generalize our computational models and novel prototype designs as feedback. Through these progressive procedures, we can pave the way for robust vigilance estimation in complex real environments. Therefore, it is very important to implement such wearable systems and test them on board vehicles.

To reduce the calibration time and improve the generalization performance of vigilance estimation models, an intuitive approach is to adaptively recycle the previously recorded data. However, there are individual differences in neurophysiological signals across subjects and sessions. The performance of vigilance estimation models may be dramatically degraded. To address this problem, one efficient approach is to perform subject transfer and session transfer using transfer learning techniques, which aim to reduce the differences of feature distributions between source domains and target domains [71]–[75].

Another similar problem is about the reality gap between simulated and real-world environments. There are many different characteristics of simulated and real scenarios. Real driving environments contain many more problems (e.g., device setups and artifacts) compared with laboratory simulations. In real-world experiments, there is usually much more noise caused by vehicle engine and vibration when recording EOG signals. However, it is very time consuming and expensive to collect a large number of high quality data in real-world environments. Therefore, an intuitive and straightforward way to dealing with this problem is to train models with data from simulations and make inference on real-world data in a cross-environment

TABLE III
PERFORMANCE COMPARISONS OF THE SAME SUBJECTS 1, 3, 5, 6, 7, AND 9 IN THE LABORATORY DRIVING SIMULATIONS AND THE REAL-WORLD DRIVING EXPERIMENTS

Subject #	Environment	COR				RMSE			
		SVR	SVR-LDS	CCRF	CCNF	SVR	SVR-LDS	CCRF	CCNF
1	Simulation	0.6753	0.6787	0.7452	0.8684	0.3067	0.2952	0.2283	0.1557
	Real	0.8926	0.8976	0.9011	0.9476	0.0969	0.0956	0.1002	0.0694
3	Simulation	0.3555	0.3586	0.3647	0.2585	0.3365	0.3348	0.3256	0.3796
	Real	0.4480	0.4518	0.5400	0.6284	0.4000	0.3943	0.2612	0.1790
5	Simulation	0.9037	0.9031	0.9020	0.9338	0.1037	0.1041	0.1051	0.0867
	Real	0.3915	0.4033	0.4407	0.1617	0.1812	0.1752	0.1381	0.1517
6	Simulation	0.8000	0.8222	0.8819	0.9026	0.1417	0.1389	0.1330	0.0988
	Real	0.4221	0.4299	0.3788	0.4039	0.1519	0.1481	0.1351	0.1440
7	Simulation	0.7191	0.7245	0.7598	0.7448	0.2756	0.2733	0.2647	0.2628
	Real	0.4884	0.5021	0.5917	0.7526	0.2441	0.2390	0.2085	0.1672
9	Simulation	0.7288	0.7440	0.7583	0.7553	0.1174	0.1158	0.1153	0.1220
	Real	0.7981	0.8006	0.7953	0.8149	0.1403	0.1389	0.1367	0.1280
Mean	Simulation	0.6971	0.7052	0.7353	0.7439	0.2136	0.2103	0.1953	0.1843
	Real	0.5735	0.5808	0.6079	0.6182	0.2024	0.1985	0.1633	0.1399
	Difference	0.1236	0.1244	0.1274	0.1257	0.0112	0.0118	0.0320	0.0444

TABLE IV
PERFORMANCE OF CROSS-ENVIRONMENT EXPERIMENTS. THE MODELS ARE TRAINED WITH THE DATA IN THE SIMULATED DRIVING ENVIRONMENT AND EVALUATED WITH THE DATA IN THE REAL-WORLD DRIVING ENVIRONMENT

Subject #	COR				RMSE			
	SVR	SVR-LDS	CCRF	CCNF	SVR	SVR-LDS	CCRF	CCNF
1	-0.2314	-0.239	-0.2831	0.8049	0.3768	0.3739	0.3501	0.1755
2	0.3528	0.3604	0.4036	0.7713	0.3298	0.3254	0.3001	0.1631
3	0.5987	0.6238	0.7105	0.0340	0.3142	0.3121	0.3076	0.3179
4	0.5410	0.5417	0.5125	0.5119	0.7211	0.7170	0.6606	0.2246
5	0.3396	0.3451	0.3689	0.4007	0.3670	0.3617	0.3323	0.1652
6	0.7204	0.7332	0.8490	0.2301	0.1425	0.1364	0.0806	0.2525
7	0.6295	0.6370	0.6705	0.5214	0.3276	0.3267	0.3228	0.3618
8	-0.3367	-0.3421	-0.4130	0.7820	0.4357	0.4333	0.4006	0.1800
9	0.8424	0.8476	0.8743	0.6717	0.1414	0.1387	0.1242	0.1751
10	-0.2539	-0.255	-0.4084	0.6680	0.2243	0.2198	0.2112	0.2462
Mean	0.3203	0.3252	0.3285	0.5396	0.3380	0.3345	0.3090	0.2262
Std	0.4374	0.4441	0.5099	0.2557	0.1664	0.1666	0.1600	0.0691

way. However, the performance of the overall systems might be dramatically degraded due to the reality gap. To address this problem, transfer learning should be further investigated for knowledge transfer from simulations to the real world and generalizing the models to real-world applications.

Compared with the EEG-based vigilance estimation approaches, EOG-based methods are much easier to implement with feasibility and wearability in real sceneries with the advantages of high amplitudes of EOGs and good placements of electrode mounting. The limitation of EOG-based vigilance estimation is that it requires a larger time window for extracting sufficient information since most eye movements such as blink and saccade are based on second scales. For example, the time window for EOG feature extraction is 8 s. In contrast, EEG signals have high temporal resolution, and they are able to capture the vigilance dynamics. In the study of Davidson *et al.* [7], they developed an EEG-based lapse detection system on the temporal scale of 4 s.

VI. CONCLUSIONS AND FUTURE WORK

For dealing with the problem of vigilance estimation in real driving environments, we have proposed both wearable device

implementations for easy signal acquisition and efficient algorithms for precise data modeling in this study. The designed wearable device has integrated only four flexible dry electrodes and a low-cost acquisition board for real-world forehead EOG recordings in comparison with the existing devices. To capture vigilance dynamics, two temporal dependency models, CCRF and CCNF, have been introduced. We have performed the systematical evaluations of our designed system in real-world driving environment under various weather conditions and validated its efficiency for continuous vigilance estimation. This study has provided an efficient approach to real-time vigilance estimation in real-world applications and the sceneries can be extended from driving tasks to various tasks that require sustained attention.

Although we have considered the weather and illumination factors and evaluated the performance under these conditions, the detailed influence of these factors in our proposed system needs systematical evaluations and further investigations with more experiments in the future. Moreover, due to the reality gap and the high cost of data collections in real scenarios, how to transfer knowledge from simulations to reality and generalize computational models to real-world applications are still open questions.

REFERENCES

- [1] S. J. Higgins *et al.*, "Asleep at the wheel—The road to addressing drowsy driving," *Sleep*, vol. 40, no. 2, p. zsx001, 2017.
- [2] M. M. Mitler, J. C. Miller, J. J. Lipsitz, J. K. Walsh, and C. D. Wylie, "The sleep of long-haul truck drivers," *New England J. Med.*, vol. 337, no. 11, pp. 755–762, 1997.
- [3] J. Smallwood *et al.*, "Subjective experience and the attentional lapse: Task engagement and disengagement during sustained attention," *Consciousness Cognition*, vol. 13, no. 4, pp. 657–690, 2004.
- [4] M. I. Posner, "Measuring alertness," *Ann. New York Acad. Sci.*, vol. 1129, no. 1, pp. 193–199, 2008.
- [5] H. H. Sievertsen, F. Gino, and M. Piovesan, "Cognitive fatigue influences students' performance on standardized tests," *Proc. Nat. Acad. Sci. USA*, vol. 113, no. 10, pp. 2621–2624, 2016.
- [6] C. Wang, J. L. Ong, A. Patanaik, J. Zhou, and M. W. Chee, "Spontaneous eyelid closures link vigilance fluctuation with fMRI dynamic connectivity states," *Proc. Nat. Acad. Sci. USA*, vol. 113, no. 34, pp. 9653–9658, 2016.
- [7] P. R. Davidson, R. D. Jones, and M. T. R. Peiris, "EEG-based lapse detection with high temporal resolution," *IEEE Trans. Biomed. Eng.*, vol. 54, no. 5, pp. 832–839, May 2007.
- [8] Q. Ji, Z. Zhu, and P. Lan, "Real-time noninvasive monitoring and prediction of driver fatigue," *IEEE Trans. Veh. Technol.*, vol. 53, no. 4, pp. 1052–1068, Jul. 2004.
- [9] B. S. Oken, M. C. Salinsky, and S. Elsas, "Vigilance, alertness, or sustained attention: Physiological basis and measurement," *Clin. Neurophysiol.*, vol. 117, no. 9, pp. 1885–1901, Sep. 2006.
- [10] E. Chua *et al.*, "Heart rate variability can be used to estimate sleepiness-related decrements in psychomotor vigilance during total sleep deprivation," *Sleep*, vol. 35, no. 3, pp. 325–334, 2012.
- [11] Y. Dong, Z. Hu, K. Uchimura, and N. Murayama, "Driver inattention monitoring system for intelligent vehicles: A review," *IEEE Trans. Intell. Transp. Syst.*, vol. 12, no. 2, pp. 596–614, Jun. 2011.
- [12] C.-T. Lin, R.-C. Wu, S.-F. Liang, W.-H. Chao, Y.-J. Chen, and T.-P. Jung, "EEG-based drowsiness estimation for safety driving using independent component analysis," *IEEE Trans. Circuits Syst. I, Reg. Papers*, vol. 52, no. 12, pp. 2726–2738, Dec. 2005.
- [13] T. O. Zander and S. Jatzev, "Context-aware brain–computer interfaces: Exploring the information space of user, technical system and environment," *J. Neural Eng.*, vol. 9, no. 1, p. 016003, 2011.
- [14] R. N. Khushaba, S. Kodagoda, S. Lal, and G. Dissanayake, "Driver drowsiness classification using fuzzy wavelet-packet-based feature-extraction algorithm," *IEEE Trans. Biomed. Eng.*, vol. 58, no. 1, pp. 121–131, Jan. 2011.
- [15] M. T. Peiris, P. R. Davidson, P. J. Bones, and R. D. Jones, "Detection of lapses in responsiveness from the EEG," *J. Neural Eng.*, vol. 8, no. 1, p. 016003, 2011.
- [16] L.-C. Shi and B.-L. Lu, "EEG-based vigilance estimation using extreme learning machines," *Neurocomputing*, vol. 102, pp. 135–143, Feb. 2013.
- [17] C.-S. Huang, N. R. Pal, C.-H. Chuang, and C.-T. Lin, "Identifying changes in EEG information transfer during drowsy driving by transfer entropy," *Frontiers Hum. Neurosci.*, vol. 9, p. 570, Oct. 2015.
- [18] D. Qian *et al.*, "Drowsiness detection by Bayesian-copula discriminant classifier based on EEG signals during daytime short nap," *IEEE Trans. Biomed. Eng.*, vol. 64, no. 4, pp. 743–754, Apr. 2017.
- [19] A. Martel, S. Dähne, and B. Blankertz, "EEG predictors of covert vigilant attention," *J. Neural Eng.*, vol. 11, no. 3, p. 035009, 2014.
- [20] C.-T. Lin, K.-C. Huang, C.-H. Chuang, L.-W. Ko, and T.-P. Jung, "Can arousing feedback rectify lapses in driving? prediction from EEG power spectra," *J. Neural Eng.*, vol. 10, no. 5, p. 056024, 2013.
- [21] S. Olbrich *et al.*, "EEG-vigilance and BOLD effect during simultaneous EEG/fMRI measurement," *Neuroimage*, vol. 45, no. 2, pp. 319–332, 2009.
- [22] L. De Gennaro, F. Vecchio, M. Ferrara, G. Curcio, P. M. Rossini, and C. Babiloni, "Antero-posterior functional coupling at sleep onset: Changes as a function of increased sleep pressure," *Brain Res. Bull.*, vol. 65, no. 2, pp. 133–140, 2005.
- [23] B. S. Oken and M. C. Salinsky, "Sleeping and driving: Not a safe dual-task," *Clin. Neurophysiol.*, vol. 118, no. 9, pp. 1899–1900, 2007.
- [24] C. Papadelis *et al.*, "Monitoring sleepiness with on-board electrophysiological recordings for preventing sleep-deprived traffic accidents," *Clin. Neurophysiol.*, vol. 118, no. 9, pp. 1906–1922, 2007.
- [25] H.-Y. Cai, J.-X. Ma, L.-C. Shi, and B.-L. Lu, "A novel method for EOG features extraction from the forehead," in *Proc. Annu. Int. Conf. IEEE Eng. Med. Biol. Soc.*, Aug. 2011, pp. 3075–3078.
- [26] X. Zhu, W.-L. Zheng, B.-L. Lu, X. Chen, S. Chen, and C. Wang, "EOG-based drowsiness detection using convolutional neural networks," in *Proc. Int. Joint Conf. Neural Netw.*, 2014, pp. 128–134.
- [27] J.-X. Ma, L.-C. Shi, and B.-L. Lu, "An EOG-based vigilance estimation method applied for driver fatigue detection," *Neurosci. Biomed. Eng.*, vol. 2, no. 1, pp. 41–51, 2014.
- [28] Y.-F. Zhang, X.-Y. Gao, J.-Y. Zhu, W.-L. Zheng, and B.-L. Lu, "A novel approach to driving fatigue detection using forehead EOG," in *Proc. 7th Int. IEEE/EMBS Conf. Neural Eng.*, Apr. 2015, pp. 707–710.
- [29] I. G. Damousis and D. Tzovaras, "Fuzzy fusion of eyelid activity indicators for hypovigilance-related accident prediction," *IEEE Trans. Intell. Transp. Syst.*, vol. 9, no. 3, pp. 491–500, Sep. 2008.
- [30] L. Zhang *et al.*, "Cognitive load measurement in a virtual reality-based driving system for autism intervention," *IEEE Trans. Affect. Comput.*, vol. 8, no. 2, pp. 176–189, Apr./Jun. 2016.
- [31] W.-L. Zheng and B.-L. Lu, "A multimodal approach to estimating vigilance using EEG and forehead EOG," *J. Neural Eng.*, vol. 14, no. 2, p. 026017, 2017.
- [32] L.-F. Wang, J.-Q. Liu, B. Yang, and C.-S. Yang, "PDMS-based low cost flexible dry electrode for long-term EEG measurement," *IEEE Sensors J.*, vol. 12, no. 9, pp. 2898–2904, Sep. 2012.
- [33] J. H. Lee, S. M. Lee, H. J. Byeon, J. S. Hong, K. S. Park, and S.-H. Lee, "CNT/PDMS-based canal-typed ear electrodes for inconspicuous EEG recording," *J. Neural Eng.*, vol. 11, no. 4, p. 046014, 2014.
- [34] H.-C. Jung *et al.*, "CNT/PDMS composite flexible dry electrodes for long-term ECG monitoring," *IEEE Trans. Biomed. Eng.*, vol. 59, no. 5, pp. 1472–1479, May 2012.
- [35] S. M. Lee *et al.*, "Self-adhesive and capacitive carbon nanotube-based electrode to record electroencephalograph signals from the hairy scalp," *IEEE Trans. Biomed. Eng.*, vol. 63, no. 1, pp. 138–147, Jan. 2016.
- [36] Y. M. Chi, T.-P. Jung, and G. Cauwenberghs, "Dry-contact and noncontact biopotential electrodes: Methodological review," *IEEE Rev. Biomed. Eng.*, vol. 3, pp. 106–119, Oct. 2010.
- [37] Y. M. Chi, Y.-T. Wang, Y. Wang, C. Maier, T.-P. Jung, and G. Cauwenberghs, "Dry and noncontact EEG sensors for mobile brain–computer interfaces," *IEEE Trans. Neural Syst. Rehabil. Eng.*, vol. 20, no. 2, pp. 228–235, Mar. 2012.
- [38] S. Ha *et al.*, "Integrated circuits and electrode interfaces for noninvasive physiological monitoring," *IEEE Trans. Biomed. Eng.*, vol. 61, no. 5, pp. 1522–1537, May 2014.
- [39] Y.-J. Huang, C.-Y. Wu, A. M.-K. Wong, and B.-S. Lin, "Novel active comb-shaped dry electrode for EEG measurement in hairy site," *IEEE Trans. Biomed. Eng.*, vol. 62, no. 1, pp. 256–263, Jan. 2015.
- [40] J. M. Rogers, S. J. Johnstone, A. Aminov, J. Donnelly, and P. H. Wilson, "Test-retest reliability of a single-channel, wireless EEG system," *Int. J. Psychophysiol.*, vol. 106, pp. 87–96, Aug. 2016.
- [41] J. Xu *et al.*, "Highly stretchable polymer semiconductor films through the nanoconfinement effect," *Science*, vol. 355, no. 6320, pp. 59–64, 2017.
- [42] C. T. Lin *et al.*, "Development of wireless brain computer interface with embedded multitask scheduling and its application on real-time driver's drowsiness detection and warning," *IEEE Trans. Biomed. Eng.*, vol. 55, no. 5, pp. 1582–1591, May 2008.
- [43] C.-T. Lin *et al.*, "Wireless and wearable EEG system for evaluating driver vigilance," *IEEE Trans. Biomed. Circuits Syst.*, vol. 8, no. 2, pp. 165–176, Apr. 2014.
- [44] T. R. Mullen *et al.*, "Real-time neuroimaging and cognitive monitoring using wearable dry EEG," *IEEE Trans. Biomed. Eng.*, vol. 62, no. 11, pp. 2553–2567, Nov. 2015.
- [45] V. Nathan and R. Jafari, "Design principles and dynamic front end reconfiguration for low noise EEG acquisition with finger based dry electrodes," *IEEE Trans. Biomed. Circuits Syst.*, vol. 9, no. 5, pp. 631–640, Oct. 2015.
- [46] A. Pinegger, S. C. Wriessnegger, J. Faller, and G. R. Müller-Putz, "Evaluation of different EEG acquisition systems concerning their suitability for building a brain–computer interface: Case studies," *Frontiers Neurosci.*, vol. 10, p. 441, Sep. 2016.
- [47] S. Ahn, T. Nguyen, H. Jang, J. G. Kim, and S. C. Jun, "Exploring neuro-physiological correlates of drivers' mental fatigue caused by sleep deprivation using simultaneous EEG, ECG, and fNIRS data," *Frontiers Hum. Neurosci.*, vol. 10, p. 219, May 2016.
- [48] T. Nguyen, S. Ahn, H. Jang, S. C. Jun, and J. G. Kim, "Utilization of a combined EEG/NIRS system to predict driver drowsiness," *Sci. Rep.*, vol. 7, Mar. 2017, Art. no. 43933.
- [49] J. A. Healey and R. W. Picard, "Detecting stress during real-world driving tasks using physiological sensors," *IEEE Trans. Intell. Transp. Syst.*, vol. 6, no. 2, pp. 156–166, Jun. 2005.

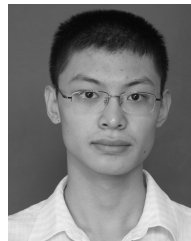
- [50] H. Wang, C. Zhang, T. Shi, F. Wang, and S. Ma, "Real-time EEG-based detection of fatigue driving danger for accident prediction," *Int. J. Neural Syst.*, vol. 25, no. 2, pp. 1550002-1-1550002-14, Mar. 2015.
- [51] H.-L. Peng, J.-Q. Liu, Y.-Z. Dong, B. Yang, X. Chen, and C.-S. Yang, "Parylene-based flexible dry electrode for biopotential recording," *Sens. Actuators B, Chem.*, vol. 231, pp. 1-11, Aug. 2016.
- [52] H.-L. Peng *et al.*, "A novel passive electrode based on porous Ti for EEG recording," *Sens. Actuators B, Chem.*, vol. 226, pp. 349-356, Apr. 2016.
- [53] G. Li, D. Zhang, S. Wang, and Y. Y. Duan, "Novel passive ceramic based semi-dry electrodes for recording electroencephalography signals from the hairy scalp," *Sens. Actuators B, Chem.*, vol. 237, pp. 167-178, Dec. 2016.
- [54] X. Guo *et al.*, "A self-wetting paper electrode for ubiquitous biopotential monitoring," *IEEE Sensors J.*, vol. 17, no. 9, pp. 2654-2661, May 2017.
- [55] Texas Instruments Inc. *Understanding Lead-Off Detection in ECG*. Accessed: Aug. 26, 2017. [Online]. Available: <http://www.ti.com/lit/an/sbaa196a/sbaa196a.pdf>
- [56] X.-Q. Huo, W.-L. Zheng, and B.-L. Lu, "Driving fatigue detection with fusion of EEG and forehead EOG," in *Proc. Int. Joint Conf. Neural Netw.*, 2016, pp. 897-904.
- [57] A. Delorme and S. Makeig, "EEGLAB: An open source toolbox for analysis of single-trial EEG dynamics including independent component analysis," *J. Neurosci. Methods*, vol. 134, no. 1, pp. 9-21, Mar. 2004.
- [58] J. Lafferty *et al.*, "Conditional random fields: Probabilistic models for segmenting and labeling sequence data," in *Proc. 18th Int. Conf. Mach. Learn. (ICML)*, vol. 1, 2001, pp. 282-289.
- [59] T. Baltrušaitis, N. Banda, and P. Robinson, "Dimensional affect recognition using continuous conditional random fields," in *Proc. 10th IEEE Int. Conf. Workshops Autom. Face Gesture Recognit.*, Apr. 2013, pp. 1-8.
- [60] T. Baltrušaitis, P. Robinson, and L.-P. Morency, "Continuous conditional neural fields for structured regression," in *Proc. Eur. Conf. Comput. Vis. Cham, Switzerland: Springer*, 2014, pp. 593-608.
- [61] J. Peng, L. Bo, and J. Xu, "Conditional neural fields," in *Proc. Adv. Neural Inf. Process. Syst.*, 2009, pp. 1419-1427.
- [62] L. M. Bergasa, J. Nuevo, M. A. Sotelo, R. Barea, and M. E. Lopez, "Real-time system for monitoring driver vigilance," *IEEE Trans. Intell. Transp. Syst.*, vol. 7, no. 1, pp. 63-77, Mar. 2006.
- [63] U. Trutschel, B. Sirois, D. Sommer, M. Golz, and D. Edwards, "PER-CLOS: An alertness measure of the past," in *Proc. 6th Int. Driving Symp. Hum. Factors Driver Assessment, Training Vehicle Design*, 2011, pp. 172-179.
- [64] X.-Y. Gao, Y.-F. Zhang, W.-L. Zheng, and B.-L. Lu, "Evaluating driving fatigue detection algorithms using eye tracking glasses," in *Proc. 7th Int. IEEE/EMBS Conf. Neural Eng.*, Apr. 2015, pp. 767-770.
- [65] M. Ferrara and L. De Gennaro, "How much sleep do we need?" *Sleep Med. Rev.*, vol. 5, no. 2, pp. 155-179, 2001.
- [66] R. H. Shumway and D. S. Stoffer, "Time series regression and exploratory data analysis," in *Time Series Analysis and its Applications*. Springer, 2011, pp. 47-82.
- [67] E. Hazan, K. Singh, and C. Zhang, "Learning linear dynamical systems via spectral filtering," in *Proc. Adv. Neural Inf. Process. Syst.*, 2017, pp. 6702-6712.
- [68] R. Talmon and R. R. Coifman, "Empirical intrinsic geometry for nonlinear modeling and time series filtering," *Proc. Nat. Acad. Sci. USA*, vol. 110, no. 31, pp. 12535-12540, 2013.
- [69] A. Natarajan, G. Angarita, E. Gaiser, R. Malison, D. Ganesan, and B. M. Marlin, "Domain adaptation methods for improving lab-to-field generalization of cocaine detection using wearable ECG," in *Proc. ACM Int. Joint Conf. Pervas. Ubiquitous Comput.*, 2016, pp. 875-885.
- [70] J. Tobin, R. Fong, A. Ray, J. Schneider, W. Zaremba, and P. Abbeel, "Domain randomization for transferring deep neural networks from simulation to the real world," in *Proc. IEEE/RSJ Int. Conf. Intell. Robots Syst.*, Sep. 2017, pp. 23-30.
- [71] S. J. Pan and Q. Yang, "A survey on transfer learning," *IEEE Trans. Knowl. Data Eng.*, vol. 22, no. 10, pp. 1345-1359, Oct. 2010.
- [72] M. Wronkiewicz, E. Larson, and A. K. Lee, "Leveraging anatomical information to improve transfer learning in brain-computer interfaces," *J. Neural Eng.*, vol. 12, no. 4, p. 046027, 2015.
- [73] H. Morioka *et al.*, "Learning a common dictionary for subject-transfer decoding with resting calibration," *NeuroImage*, vol. 111, pp. 167-178, May 2015.
- [74] Y.-Q. Zhang, W.-L. Zheng, and B.-L. Lu, "Transfer components between subjects for EEG-based driving fatigue detection," in *Proc. Int. Conf. Neural Inf. Process. Cham, Switzerland: Springer*, 2015, pp. 61-68.

- [75] W.-L. Zheng and B.-L. Lu, "Personalizing EEG-based affective models with transfer learning," in *Proc. Int. Joint Conf. Artif. Intell.*, 2016, pp. 2732-2738.



Wei-Long Zheng (S'14) received the bachelor's degree in information engineering from the Department of Electronic and Information Engineering, South China University of Technology, Guangzhou, China, in 2012, and the Ph.D. degree in computer science from the Department of Computer Science and Engineering, Shanghai Jiao Tong University, Shanghai, China, in 2018. He received the IEEE TRANSACTIONS ON AUTONOMOUS MENTAL DEVELOPMENT Outstanding Paper Award from the IEEE Computational Intelligence Society in 2018.

His research interests focus on affective computing, brain-computer interaction, machine learning, and pattern recognition.

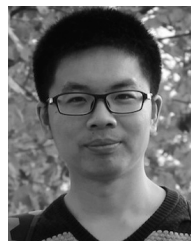


Kungpeng Gao is currently pursuing the Ph.D. degree with the Department of Micro/Nano Electronics, Shanghai Jiao Tong University, Shanghai, China. His research interests focus on microelectromechanical systems, biomedical microsystems, and micro/nano fabrication technology.



Gang Li received the B.E. degree in communication engineering from Nanchang Hangkong University, Nanchang, China, in 2007, the M.S. degree in computer engineering from Pusan National University, in 2010, and the Ph.D. degree in electronic engineering from Pukyong National University, Busan, South Korea, in 2016. He was a Visiting Scholar with the Neuroscape Center, University of California, San Francisco, USA. He is currently a Research Associate with Shanghai Jiao Tong University, China. His current research interest is

EEG-VR-based cognitive neuroscience.



Wei Liu received the bachelor's degree in automation from the Department of Automation Science and Electrical Engineering, Beihang University, Beijing, China, in 2014. He is currently pursuing the Ph.D. degree in computer science with the Department of Computer Science and Engineering, Shanghai Jiao Tong University, Shanghai, China. His research interests focus on affective computing, brain-computer interface, and machine learning.



Chao Liu received the bachelor's degree in computer science from the Department of Computer Science and Engineering, Shanghai Jiao Tong University, Shanghai, China, in 2016. His research interests include affective computing, machine learning, and EEG-based vigilance estimation.



Jing-Quan Liu was born in Jilin, China, in 1971. He received the Ph.D. degree from Jilin University, Changchun, China, in 2000.

From 2006 to 2007, he was a Visiting Scholar with the Department of Electrical Engineering, California Institute of Technology, Pasadena. He is currently a Professor with the Institute of Micro/Nano Science and Technology, Shanghai Jiao Tong University, Shanghai, China. His current research interests include MEMS, biomedical microsystems, and micro/nano fabrication technology.



Guoxing Wang (M'06–SM'13) received the Ph.D. degree in electrical engineering from the University of California at Santa Cruz, Santa Cruz, CA, USA, in 2006.

He was a Member of Technical Staff with Agere Systems Inc., San Jose, CA, USA, from 2006 to 2007. From 2007 to 2009, he was with the Second Sight Medical Products, Sylmar California, where he designed the integrated circuits chip that went into the eyes of patients to restore vision. He is currently an Associate Professor with the School of

Microelectronics, Shanghai Jiao Tong University, Shanghai, China. He has published many papers in various peer-reviewed journals and in various conferences. His current research interests include biomedical electronics, and bio-inspired circuits and systems.

Dr. Wang currently serves as the Deputy Editor-in-Chief for the *IEEE TRANSACTIONS ON BIOMEDICAL CIRCUITS AND SYSTEMS* (2016–2019). He is a member of the IEEE Biomedical Circuits Systems Technical Committee. He served as an Associate Editor for the *IEEE TRANSACTIONS ON CIRCUITS AND SYSTEMS II* (2012–2015), and as the Guest Editor for the *IEEE JOURNAL ON EMERGING AND SELECTED TOPICS IN CIRCUITS AND SYSTEMS* and the *IEEE TRANSACTIONS ON BIOMEDICAL CIRCUITS AND SYSTEMS*, both in 2014. He served as the Technical Program Chair for the *IEEE Conference on Biomedical Circuits and Systems* in 2016. He was the Local Chair of the first IEEE Green Circuits and Systems, in 2010, and the second Asia Pacific Conference on Postgraduate Research in Microelectronics and Electronics (PrimeAsia) in 2010.



Bao-Liang Lu (M'94–SM'01) received the B.S. degree in instrument and control engineering from the Qingdao University of Science and Technology, Qingdao, China, in 1982, the M.S. degree in computer science and technology from Northwestern Polytechnical University, Xi'an, China, in 1989, and the Dr.Eng. degree in electrical engineering from Kyoto University, Kyoto, Japan, in 1994.

He was with the Qingdao University of Science and Technology from 1982 to 1986. From 1994 to 1999, he was a Frontier Researcher with the Bio-Mimetic Control Research Center, Institute of Physical and Chemical Research (RIKEN), Nagoya, Japan, and a Research Scientist with the RIKEN Brain Science Institute, Wako, Japan, from 1999 to 2002. Since 2002, he has been a Full Professor with the Department of Computer Science and Engineering, Shanghai Jiao Tong University, Shanghai, China. He received the IEEE TRANSACTIONS ON AUTONOMOUS MENTAL DEVELOPMENT Outstanding Paper Award from the IEEE Computational Intelligence Society in 2018. His current research interests include brain-like computing, neural networks, machine learning, brain-computer interaction, and affective computing.

Prof. Lu is currently a Board Member of the Asia Pacific Neural Network Society (APNNS, previously APNNA) and the Steering Committee member of the *IEEE TRANSACTIONS ON AFFECTIVE COMPUTING*. He was the President of the Asia Pacific Neural Network Assembly (APNNA) and the General Chair of the 18th International Conference on Neural Information Processing in 2011. He is currently the Associate Editor of the *IEEE TRANSACTIONS ON COGNITIVE AND DEVELOPMENT SYSTEMS*.